




All-Optical QPSK Pattern Recognition in High-Speed Optoelectronic Firewalls

Qihan Zhang , Member, IEEE, Xiaoxue Gong , and Lei Guo 

Abstract—In the 5G era, more sensitive information will be transmitted on optical networks. Although modern cryptography could support different security mechanisms in different layers, the optical layer has not been paid enough attention but it is also vulnerable to attack by tapping or other methods. The optoelectronic firewall is one of the promising security strategies which can accelerate the operating speed within manageable costs by employing optical signal processing compared with current electronic firewalls. The most significant and challenging component of an optoelectronic firewall is pattern recognition. However, either the latest pattern recognition systems can only process the OOK or BPSK modulation format signals, or the coherent correlators supporting higher order modulation format require advanced components to deal with a higher number of symbols. In this paper, to address the pattern recognition challenges, we propose, analyze and simulate a pattern recognition system of QPSK signals integrated into all-optical high-speed optoelectronic firewalls used for optical layer security. The numerical simulation results first demonstrate the feasibility, and a baud rate of 100GBaud can be achieved. Next, a threshold-setting method is developed which also proves the ability to recognize arbitrary target patterns. Then some noise analysis results demonstrate that the pattern recognition of the I branch can be immune to the noise while the output power of EDFAs in the Q branch needs to be configured carefully. Finally, the matched result of a real Ethernet frame further reveals that our proposed system is promisingly applied in optoelectronic firewalls.

Index Terms—Optoelectronic firewall, pattern recognition, four-wave mixing (FWM), format conversion, optical logic, optical correlator.

Manuscript received 28 December 2022; revised 31 January 2023; accepted 6 February 2023. Date of publication 10 February 2023; date of current version 21 February 2023. This work was supported in part by the National Nature Science Foundation of China under Grants 62075024, 62201105, 62205043, 62025105, and 62071076, in part by the Nature Science Foundation of Chongqing under Grants CSTB2022NSCQ-MSX1334 and cstc2021jcyj-msxmX0404, in part by the Chongqing Municipal Education Commission under Grants CXQT21019 and KJQN202100643, in part by the China Postdoctoral Science Foundation under Grant 2021M700563, and in part by the Chongqing Postdoctoral Funding Project under Grant 2112012727685993. (Corresponding author: Xiaoxue Gong.)

Qihan Zhang is with the School of Computer Science and Engineering, Northeastern University, Shenyang, Liaoning 110819, China, and also with the Institute of Intelligent Communication and Network Security, Chongqing University of Posts and Telecommunications, Chongqing 400065, China (e-mail: qihanzhang@stumail.neu.edu.cn).

Xiaoxue Gong and Lei Guo are with the School of Communication and Information Engineering, Chongqing University of Posts and Telecommunications, Chongqing 400065, China, and also with the Institute of Intelligent Communication and Network Security, Chongqing University of Posts and Telecommunications, Chongqing 400065, China (e-mail: gongxx@cqupt.edu.cn; guolei@cqupt.edu.cn).

Digital Object Identifier 10.1109/JPHOT.2023.3243896

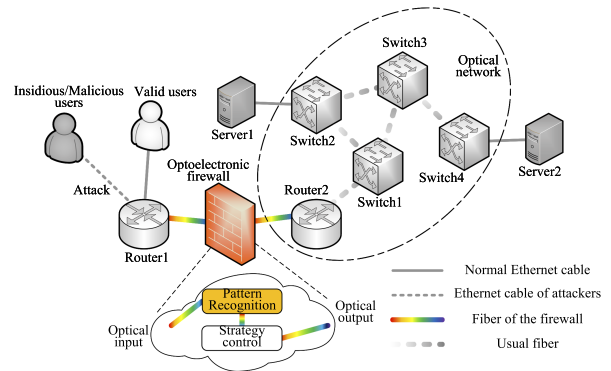


Fig. 1. Location of the optoelectronic firewall in an optical network.

I. INTRODUCTION

OPTICAL networks support emerging bandwidth-hungry services such as Ultra/Super High-Definition Video streaming (4K/8K video), Virtual Reality/Augmented Reality (VR/AR), Autonomous Vehicle (AV), and robotics in the 5G era. Inevitably, more sensitive information such as financial transactions, medical records, and confidential intellectual property [1] will be transmitted on them. Although various security mechanisms are used to protect the confidentiality, integrity, and availability triad supported by modern cryptography in the application layer (e.g. Secure Shell, SSH), transport layer (e.g. Transport Layer Security, TLS), network layer (e.g. Internet Protocol Security, IPSec) and data link layer (e.g. Layer 2 Tunneling Protocol, L2TP), security protection in the optical layer has not been attracting much attention. However, the optical layer is also vulnerable to attack by tapping [1], [2], [3], listening to the residual adjacent channel crosstalk [2], in-band jamming, and out-of-band crosstalk [3] without any destruction of the communication systems. For decades, the ceaseless pursuit of balancing the contradiction between large capacity and high security in the optical layer never stops, resulting in plenty of technologies such as encryption using all-optical logic gates [4], optical steganography [5], chaotic laser [6], optoelectronic firewall [7], and other passive or active approaches to cope with the security threats of the optical layer. As an active method to guarantee security, the optoelectronic firewall technology can eliminate some classes of insidious and malicious traffic, only allowing wanted traffic to transmit. The location of an optoelectronic firewall for an optical network to be protected is illustrated in Fig. 1.

Actually, a current electronic firewall could be integrated at the critical node such as Router2 in Fig. 1. However, for modern 100/400 Gbps optical links or the next-generation requirements, an electronic firewall needs so expensive and high power-consuming Optical-Electrical-Optical conversion to support that is too complicated to handle data rates approaching 1Tbps [7]. The optical signal processing technology can dramatically accelerate the operating speed within manageable costs, hence, implementing an optoelectronic firewall in the optical domain as shown in Fig. 1 can offer advantages over electronics and potentially achieve the 1Tbps-security target.

An optoelectronic firewall generally consists of two components as Fig. 1 illustrates: pattern recognition for wanted or unwanted traffic and strategy control according to the recognition results. Pattern recognition, identifying a specific target pattern sequence from the optical input signal, is the most significant and challenging component of an optoelectronic firewall. Now there are two main ways to achieve pattern recognition. One is constructed by all-optical logic gates, for example, XNOR/XOR and AND in [8] and [9] (the latest approaches). These kinds of pattern recognition systems can be easy to achieve high bit rates up to 160Gps and 200 Gbps respectively and recognize arbitrary target patterns, however, the modulation format of input data must be On-Off Keying (OOK) or Binary Phase Shift Keying (BPSK). The other is implemented by coherent correlators, for example, employing Orbital Angular Momentum (OAM) mode delays [10], Periodically-Poled-Lithium-Niobate (PPLN) waveguide [11], and cascaded Mach-Zehnder interferometers (MZIs) [12] (the latest approaches). These systems can recognize the modulation format of Quadrature Phase Shift Keying (QPSK) and achieve high data rates up to 100 Gbps, however, more OAM modes or MZIs [10], [12], PPLN waveguides with high conversion efficiency and advanced coherent receivers would be required to deal with a higher number of symbols [13].

To address the above-mentioned technical challenges, especially for arbitrary pattern recognition of high-order modulation format, a complete QPSK recognition system that could recognize the In-Phase (I) branch and the Quadrature (Q) branch simultaneously is proposed in this work. The proposed system combines the advantages of both high-speed arbitrary target pattern recognition of all-optical logic gates and high order modulation format of coherent correlators by employing the Four Wave Mixing (FWM) effect over Highly Non-Linear Fibers (HNLFs). Our previous work [14], [15] has preliminarily investigated the recognition of the I branch. In this work, more details have been elaborated for the recognition of the I branch and the recognition of the Q branch is integrated. The contributions of this proposed system in this paper are summarized as follows:

- For optical layer security, we propose a novel all-optical system for the pattern recognition of high-order modulation format of QPSK signals.
- For the format conversion process of the Q branch in our proposed system, we redesign a similar system with unequally spaced frequencies instead of equidistant pumps to improve the flexibility of the frequency conversion. To understand the unequally spaced operating principle of our

redesign, we develop a more general explanation than that of current similar systems.

- Different from adding $\pi/2$ -shift method to implement format conversion of the I branch with the same structure of the Q branch, we design a phase-insensitive method of the I branch's format conversion which can save half of the phase-locking circuits format.
- The numerical simulation results demonstrate that our system can recognize arbitrary target patterns at a baud rate of up to 100 GBaud, which describes 200 Gbps that is expected to achieve large-scale commercial deployment in the 5G era of source QPSK signals.
- There are three advantages of the proposed system that could reduce the cost and requirement of the real experiment implementation in the future as follows. First, only commercial HNLFs without any custom parameters are needed for each FWM process. Then, all processes could be achieved by shelf optical components. Finally, as far as the output of the recognition results in the I and Q branch, a simple PIN photodiode (PD) rather than a complex coherent receiver is needed.

The rest of this paper is organized as follows. In Section II, we make an extensive survey on all-optical pattern recognition and optoelectronic firewall technologies for optical layer security in the recent two decades. An elaborate theoretical derivation for the operating principle of the proposed system is analyzed in Section III. We configure the numerical simulation conditions and simulation setup in Section IV. The system performance results are discussed in Section V before concluding this paper in Section VI.

II. RELATED WORK

All-optical pattern recognition can recognize the address and port number of an input signal, which is not only applicable for optical packet switching but also for data security applications such as optoelectronic firewalls [16].

To process optical packets on the fly, Martinez et al. [17] proposed a novel recognition scheme using SOA-based Mach-Zehnder interferometer (SOA-MZI) to implement cascaded XOR logic gates for 2-bit pattern recognition from 10 Gbps optical labels. Aljada et al. [18] even used a reconfigurable dedicated Opto-VLSI processor to recognize 4-, 6- and 8-bit patterns in dynamic 10 Gbps WDM headers/labels. For higher processing speed during the pattern recognition, a simplified Vander Lugt correlator [19] implemented by a 20 km single-mode fiber, a Phase Modulator (PM), and a dispersion-compensation module was proposed and demonstrated to recognize a 4-bit pattern from 100 Gbps optical packet headers and the design could be scaled up for 8-bit headers recognition at 1Tbps as the authors claimed.

Note that the modulation format of the input signals in pattern recognition methods mentioned previously are all OOK (Intensity Modulation, IM, or Pulse Amplitude Modulation, PAM is essentially the same), which must be upgraded to phase modulation or high order modulation like Binary Phase Shift Keying (BPSK), QPSK, 8 Phase Shift Keying (8PSK) and

Quadrature Amplitude Modulation (QAM) in the next generation all-optical networks for larger transmission capacity, Cincotti [20] proposed a novel tree of unbalanced MZIs architecture to perform correlations in parallel for 100 Gbps label processing with the modulation format of BPSK or 8PSK. To suppress the noise more effectively in Cincotti's architecture, Moriwaki et al. [21] proposed another correlator based on silica-based Planar Lightwave Circuit (PLC) and a unique label format for the 4-bit recognition from a 40 Gbps stream. An 8-bit passive or programmable correlator also at 40 Gbps used for BPSK signals was demonstrated by employing a high-index-contrast silica-on-silicon PLC according to Kand et al. [22], [23], scaling up the length of the target pattern. Kibria et al. [24] proposed a correlation technique using both IM and PM of the signal wavelengths based on the FWM effect over an HNLFF by converting different wavelengths into the same wavelength at 10 Gbps for 4-bit pattern recognition.

In 2006, a project believed to be the first to tackle security issues in packet-based networks [7] named Wirespeed Security Domains using Optical Monitoring (WISDOM) [25] was launched, aiming to develop advanced optical components necessary for optoelectronic firewalls, which includes operations such as optical packet recognition, interrogation and manipulating data streams incorporating features of parity checking, flag status, and header recognition. [7] is the most representative. The authors proposed an innovative circular matching structure integrated with XNOR, AND, and regenerator implemented by SOA-MZIs. The results revealed that the structure could recognize the arbitrarily chosen OOK target patterns ranging in length from 8 to 256 bits from 42.6 Gbps optical packet headers. Up to now, as a continuation of [7], Guo et al. [26] replaced the XNOR with XOR and achieved up to 32-bit pattern recognition from a 128-bit 40 Gbps OOK signal. To solve the time-consuming and inefficient circular matching, a parallel recognition structure was designed in [27] for short target pattern and achieved 8-bit recognition from 128-bit 40 Gbps OOK signal. For higher processing speed, Liu et al. [8] replaced all SOAs with HNLFFs and redesigned the XOR into two opposite processes with the help of the Cross-Phase Modulation (XPM) effect. Simulation results revealed that an 8-bit target pattern could be recognized from a 64-bit 160 Gbps OOK signal. Xu et al. [9] integrated three similar structures implemented by HNLFFs of [7] to recognize the target sequence with the length of k times. They showed that an 8-bit pattern can be recognized from a 100 Gbps or 200 Gbps BPSK sequence. However, whether the proposed structure can be suitable for high order modulation format has not been reported.

As for the higher-order modulation format of QPSK, Willner's team has to be mentioned. Chitgarha et al. [28] started the study of simultaneous correlation for QPSK signals and equalization for QPSK, 8PSK, and 16QAM by employing $\chi^{(2)}$ nonlinear processes in two PPLN waveguides and an Optical Frequency Comb (OFC) to recognize the 4-symbol pattern from a 1000-symbol 40 Gbps QPSK signal. A similar system has been implemented in [13] and [29] by replacing the generation of OFC with a mode-locked laser followed by delay line interferometer

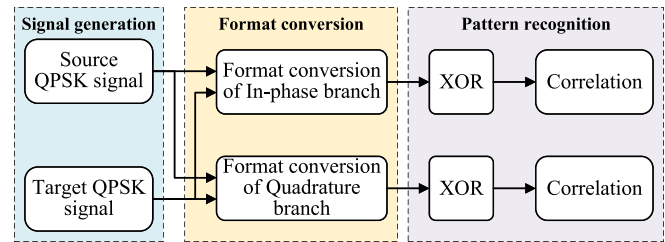


Fig. 2. General architecture of the QPSK pattern recognition system.

and HNLFF or an integrated microresonator, and 6- or 3-symbol pattern could be recognized from 4096- or 1000-symbol 40 Gbps QPSK signal, respectively. Considering that correlation nodes may be located at a distance from the transmitter and without access to optical sources, Alishahi et al. [11] demonstrated a remote tunable optical correlator with a structure similar to [28] for recognizing the 2-symbol pattern from a 20-30 Gbps QPSK signal. Other approaches such as employing the cascaded MZIs or OAM mode delays are also demonstrated in [12] and [10], where the number of the recognized pattern can be up to 4- or 3-symbol with the data rate up to 100 Gbps or 40 Gbps. Nevertheless, none of the three approaches with PPLN waveguides, MZIs, or OAM mode delays to implement the coherent correlators have reported the pattern recognition of more than 6 symbols. If more symbol patterns were desired, high efficiency of PPLN waveguides [13], more MZIs, more OAM modes [10] or even advanced coherent receivers would be required as the references claimed, which is more expensive and complicated.

In conclusion, although the latest pattern recognition systems can be easy to achieve high bit rates and recognize arbitrary target patterns, the modulation format of input data must be OOK. The high-order modulation format pattern recognition systems can recognize the modulation format of QPSK, however, the number of patterns is too expensive or complicated to be recognized more than 6 symbols. For increasing security threats in the optical layer, there is an urgent need for a system combining the advantages of both high-speed arbitrary target pattern recognition of all-optical logic gates and high order modulation format of coherent correlators, which is exactly the system we propose in this work.

III. OPERATING PRINCIPLE

In this section, we first introduce the general architecture and basic assumptions of our proposed system. We then analyze the operating principle in an elaborate theoretical derivation of each structure.

A. General Architecture and Basic Assumptions

Fig. 2 illustrates the general architecture of our proposed system. It consists of three cascaded parts: signal generation of a source QPSK signal and a target pattern QPSK signal to be recognized, format conversion from QPSK to BPSK of I branch and Q branch by employing FWM over HNLFFs and pattern recognition process of source and target patterns. Here,

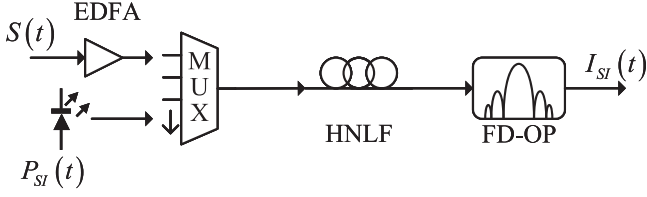


Fig. 3. Format conversion structure of I branch.

the format conversion is the most innovative and complicated part, and to a certain extent, it decides how to generate the source and target QPSK signal. As a result, we elaborate on the process of format conversion in different branches at first. Then we design the signal generation process. Finally, the principle of the pattern recognition process will be explained.

To analyze the main processes in the proposed system, it is necessary to give the following basic definitions, assumptions, and approximations. Firstly, for the signals' forward propagation along the HNLF, we take the beginning of the fiber as the origin and establish a coordinate system along the propagation direction of the optical field using the coordinate z . Secondly, under the quasi-continuous-wave conditions, the time dependence of the signals is neglected so that the dispersion-related term in the fiber's non-linear Schrodinger equation could be ignored. Thirdly, although FWM is a polarization-sensitive effect, we assume that all input signals at the beginning are aligned with the fast axis (X axis) linear part of the polarization to find the approximate solution analytically from the complex Coupled Amplitude Equations (CAEs). Finally, since the peak powers of the incident pumps to stimulate FWM are usually high enough, stimulated inelastic scattering such as Stimulated Raman Scattering (SRS) and Stimulated Brillouin Scattering (SBS) could be generated. We take no account of their influence here because SBS is extremely weak in the forward direction in HNLF [30] and several methods have the potential to mitigate the effect as mentioned in [31]. As for SRS, we use the common values of SRS for the HNLF model in VPI simulation to verify its effect in Section V. It turns out that SRS has little effect on the pattern recognition results, therefore, the assumption of taking no consideration of SRS and SBS is correct.

B. Format Conversion

All structures of format conversion even in different branches are composed of an FWM operation and a filter followed by the details of the I branch shown in Fig. 3 and the Q branch shown in Fig. 6. The difference is the number of input pumps and the center frequency of the filter.

1) *Format Conversion of I Branch*: As shown in Fig. 3, suppose the source QPSK signal at $z = 0$ is described as $S(0, t) = S(t) = A_s \exp[j(2\pi f_c t + \varphi_{QPSK_s})]$, where A_s is the amplitude, f_c is the center frequency, φ_{QPSK_s} is the QPSK phase and $\varphi_{QPSK_s} \in \{\pi/4, 3\pi/4, -3\pi/4, -\pi/4\}$. A degenerate FWM (DFWM) process [32] is stimulated by amplifying $S(0, t)$ through an Erbium-Doped Fiber Amplifier (EDFA)

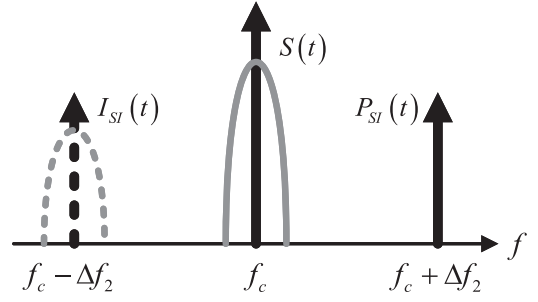


Fig. 4. Frequency allocation during the DFWM of I branch's format conversion.

over an HNLF fed with an input pump $P_{SI}(0, t) = P_{SI}(t) = A_{psi} \exp\{j[2\pi(f_c + \Delta f_2)t + \varphi_{Pump_{psi}}]\}$, where A_{psi} is the amplitude and $\varphi_{Pump_{psi}}$ is the initial phase, Δf_2 describes the difference of the center frequency between $S(0, t)$ and $P_{SI}(0, t)$ by a multiplexer (MUX). A desired idle signal at frequency $2f_c - (f_c + \Delta f_2) = f_c - \Delta f_2$ described as $I_{SI}(z, t)$ will be generated after the DFWM process as Fig. 4 illustrates. Then $S(z, t)$, $P_{SI}(z, t)$ and $I_{SI}(z, t)$ should satisfy a CAEs given by [30]:

$$\begin{cases} \frac{dS}{dz} = j\gamma_{SI} |S|^2 S \\ \frac{dP_{SI}}{dz} = j\gamma_{SI} (2|S|^2 P_{SI} + S^2 \overline{I_{SI}} e^{-j\Delta k_{SI} z}) \\ \frac{dI_{SI}}{dz} = j\gamma_{SI} (2|S|^2 I_{SI} + S^2 \overline{P_{SI}} e^{-j\Delta k_{SI} z}) \end{cases} \quad (1)$$

In (1), assume that the power of $S(z, t)$ is much larger than that of $P_{SI}(z, t)$ or $I_{SI}(z, t)$, i.e., $|S|^2 \gg |P_{SI}|^2$ or $|I_{SI}|^2$ and the initial value of $I_{SI}(z, t)$ is 0, i.e., $I_{SI}(0, t) = 0$. γ_{SI} is the nonlinear parameter of the HNLF, $\Delta k_{SI} = \beta_{P_{SI}} + \beta_{I_{SI}} - 2\beta_S$ is the mismatch of the input signals' mode-propagation constant β_S , $\beta_{P_{SI}}$ and that of output signal $\beta_{I_{SI}}$. According to the assumptions and parameters description above, the solution of (1) can be solved as [33]:

$$\begin{cases} S(z, t) = S(0, t) e^{j\gamma_{SI} |S|^2 z} \\ P_{SI}(z, t) = P_{SI}(0, t) \left[\cosh(g_{SI} z) + j \frac{\kappa_{SI}}{2g_{SI}} \sinh(g_{SI} z) \right] e^{j(2\gamma_{SI} |S|^2 - \kappa_{SI}/2) z} \\ I_{SI}(z, t) = j \frac{\gamma_{SI}}{g_{SI}} [S(0, t)]^2 \overline{P_{SI}(0)} \sinh(g_{SI} z) \cdot e^{j(2\gamma_{SI} |S|^2 - \kappa_{SI}/2) z} \\ = \frac{\gamma_{SI}}{g_{SI}} A_s^2 \sinh(g_{SI} z) e^{j(2\gamma_{SI} |S|^2 - \kappa_{SI}/2) z} \cdot e^{j[2\pi(f_c - \Delta f_2)t + (2\varphi_{QPSK_s} + \pi/2 - \varphi_{Pump_{psi}})]} \end{cases} \quad (2)$$

where $\kappa_{SI} = 2\gamma_{SI} |S|^2 + \Delta k_{SI}$ and $g_{SI} = \sqrt{\gamma_{SI}^2 |S|^4 - (\kappa_{SI}/2)^2}$.

The phase of $2\varphi_{QPSK_s} + \pi/2$ in $I_{SI}(z, t)$ of (2) means that the phase of $I_{SI}(z, t)$ will change to $\varphi_{BPSK_s} = 2\varphi_{QPSK_s} + \pi/2 \in \{\pi, 0, \pi, 0\}$ after the DFWM process, this could be considered as a BPSK signal with two discrete phases. To illustrate the above-mentioned phase change in the DFWM process, Fig. 5 shows the constellation conversion of $I_{SI}(z, t)$. The constellation of φ_{QPSK_s} in four white solid circles is firstly doubled and

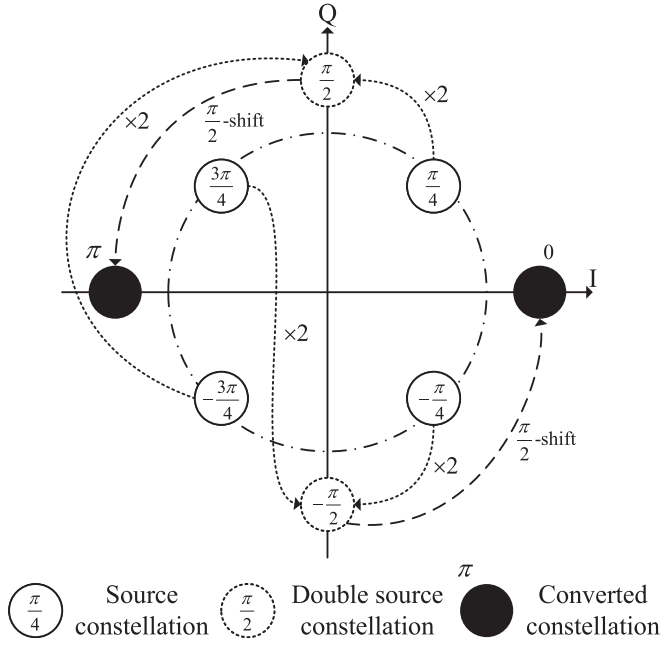


Fig. 5. Constellation conversion from QPSK to BPSK of I branch [i.e., $S(0, t) \rightarrow I_{SI}(z, t)$].

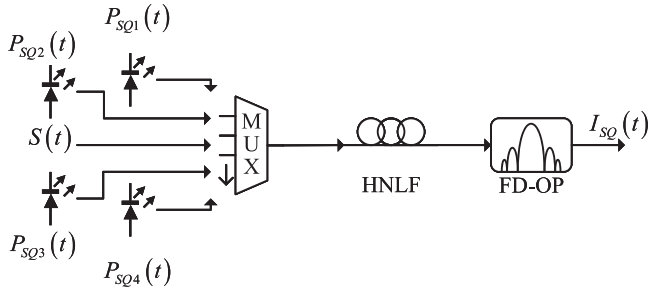


Fig. 6. Format conversion structure of Q branch.

changed to the position in two white dashed circles. Then they are shifted $\pi/2$ to the position in black solid circles.

Note that the DFWM process is easy to be configured since no pump requires phase locking like Section III-B2. Therefore, the proposed structure for format conversion of the I branch has implementation advantages. After the DFWM process, the output signal of the HNLF will be made up of $S(z, t)$, $P_{SI}(z, t)$ and $I_{SI}(z, t)$. The desired $I_{SI}(z, t)$ indicating the converted BPSK signal need to be filtered. In this work, Frequency-Domain Optical Processors (FD-OPs) like [34] are adopted to be the tunable filters due to too many frequencies participating in the FWM processes. There needs a simple method to be able to configure the arbitrary center frequencies, bandwidths, and shapes of the filters during different FWM processes to achieve better performance for the filtered signals. An FD-OP can be exactly programmed to implement this method. Hence, we filter $I_{SI}(z, t)$ and reformulate the output signal as $I_{SI}(t)$ by an FD-OP to obtain the BPSK signal preparing for the next pattern recognition process.

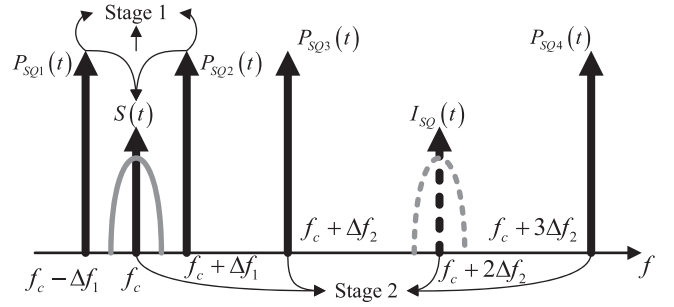


Fig. 7. Frequency allocation and two simultaneous stages in Q branch's format conversion.

2) *Format Conversion of Q Branch:* As shown in Fig. 6, an FWM process is stimulated by four phase-locked high power pumps described as:

$$P_{SQx}(0, t) = P_{SQx}(t) = \begin{cases} A_{psqx} e^{j\{2\pi[f_c + (2x-3)\Delta f_1]t + \varphi_{Pumpsqx}\}}, & x \in \{1, 2\} \\ A_{psqx} e^{j\{2\pi[f_c + (2x-5)\Delta f_2]t + \varphi_{Pumpsqx}\}}, & x \in \{3, 4\} \end{cases} \quad (3)$$

where A_{psqx} , $\varphi_{Pumpsqx}$, $(2x-3)\Delta f_1$ and $(2x-5)\Delta f_2$ have the same meaning of that in $P_{SI}(0, t)$ with the phase-locked $S(0, t)$. The generation of these phase-locked pumps has nothing to do with the analysis of format conversion in this section, we will elaborate on the phase-locking subsystem in Section IV-A.

Obviously, the five-input FWM is too complex to satisfy the general CAEs because of the participation of two more pumps. Previously, [31], [35], [36], [37] have experimentally demonstrated that this type of FWM process can convert the I and Q branch of QPSK format to BPSK format and simultaneous frequency conversion by employing the nonlinear media SOA, HNLF or PPLN waveguide. However, the previous work was all based on equidistant pumps, which made the frequency conversion inflexible to any expected frequency. Therefore, in this work, we redesign a similar format conversion system with unequally spaced frequencies to improve the flexibility of the arbitrary frequency conversion. Although Webb et al. and Baillot et al. even managed to explain the principles of their conversion in [38] and [39], respectively, the principles are neither applicable to the HNLFs (Webb's principle) nor the unequally spaced pumps (Baillot's principle). To thoroughly understand the details of this unequally spaced pumps' FWM process, we divide the whole FWM process into two simultaneous stages similar to the treatment method in [40]. The first stage named Stage 1 is a DFWM process that can convert the signal from QPSK to BPSK in the same wavelength. The second stage called Stage 2 is a usual FWM process that copies the converted BPSK signal to another wavelength to be applied in the next pattern recognition process. Fig. 7 illustrates the frequency allocation and the two simultaneous stages in Q branch format conversion.

a) *Stage 1:* According to Fig. 7, at the first stage, a DFWM is stimulated by the phase-locked $P_{SQ1}(0, t)$ and $P_{SQ2}(0, t)$ with $S(0, t)$. Therefore, $P_{SQ1}(z, t)$, $P_{SQ2}(z, t)$ and $S(z, t)$

should satisfy the CAEs expressed as:

$$\begin{cases} \frac{dP_{SQ1}}{dz} = j\gamma_{SQ1} \left[\left(|P_{SQ1}|^2 + 2|P_{SQ2}|^2 \right) P_{SQ1} \right] \\ \frac{dP_{SQ2}}{dz} = j\gamma_{SQ1} \left[\left(|P_{SQ2}|^2 + 2|P_{SQ1}|^2 \right) P_{SQ2} \right] \\ \frac{dS}{dz} = j2\gamma_{SQ1} \left[\left(|P_{SQ1}|^2 + |P_{SQ2}|^2 \right) S + P_{SQ1}P_{SQ2}\bar{S}e^{-j\Delta k_{SQ1}z} \right] \end{cases} \quad (4)$$

In (4), except for the description of γ_{SQ1} , assume that $|P_{SQ1}|^2$ or $|P_{SQ2}|^2 \gg |S|^2$ and $\Delta k_{SQ1} = 2\beta_S - \beta_{P_{SQ1}} - \beta_{P_{SQ2}}$. According to the same method for solving (1), the solution of (4) can be solved as:

$$\begin{cases} P_{SQ1}(z, t) = P_{SQ1}(0, t) e^{j\gamma_{SQ1}(|P_{SQ1}|^2 + 2|P_{SQ2}|^2)z} \\ P_{SQ2}(z, t) = P_{SQ2}(0, t) e^{j\gamma_{SQ1}(|P_{SQ2}|^2 + 2|P_{SQ1}|^2)z} \\ S(z, t) = \left\{ S(0, t) \left[\cosh(g_{SQ1}z) + j\frac{\kappa_{SQ1}}{2g_{SQ1}} \cdot \sinh(g_{SQ1}z) \right] + j\frac{2\gamma_{SQ1}}{g_{SQ1}} P_{SQ1}(0, t) \cdot P_{SQ2}(0, t) \bar{S}(0, t) \sinh(g_{SQ1}z) \right\} \cdot e^{j[2\gamma_{SQ1}(|P_{SQ1}|^2 + |P_{SQ2}|^2) - \kappa_{SQ1}/2]z} \end{cases} \quad (5)$$

where $\kappa_{SQ1} = \gamma_{SQ1}(|P_{SQ1}|^2 + |P_{SQ2}|^2) + \Delta k_{SQ1}$ and

$g_{SQ1} = \sqrt{4\gamma_{SQ1}^2|P_{SQ1}|^2|P_{SQ2}|^2 - (\kappa_{SQ1}/2)^2}$. It is hard to make $S(z, t)$ out from the expression in (5). Note that when the DFWM process of (5) is stimulated, κ_{SQ1} should be small enough and close to zero, i.e., $\kappa_{SQ1} \approx 0$, which leads $g_{SQ1} \approx 2\gamma_{SQ1}|P_{SQ1}||P_{SQ2}|$. Substitute the approximate value of κ_{SQ1} and g_{SQ1} into $S(z, t)$ in (5). $S(z, t)$ can be approximated as (6).

$$\begin{aligned} S(z, t) \approx & \left[A_s e^{j(2\pi f_c t + \varphi_{QPSKs})} \cosh(g_{SQ1}z) \right. \\ & \left. + jA_s e^{j(2\pi f_c t + \varphi_{C1} - \varphi_{QPSKs})} \sinh(g_{SQ1}z) \right] \cdot \\ & e^{j[2\gamma_{SQ1}(|P_{SQ1}|^2 + |P_{SQ2}|^2) - \kappa_{SQ1}/2]z} \end{aligned} \quad (6)$$

where $\varphi_{C1} = \varphi_{Pumpsq1} + \varphi_{Pumpsq2}$ is a constant since the input pumps $P_{SQ1}(0, t)$, $P_{SQ2}(0, t)$ and the signal $S(0, t)$ are phase-locked. Here, suppose $\varphi_{C1} = \pi/2$, (6) can be further simplified as:

$$\begin{aligned} S(z, t) = & \left[A_s e^{j(2\pi f_c t + \varphi_{QPSKs})} \cosh(g_{SQ1}z) \right. \\ & \left. + jA_s e^{j(2\pi f_c t + \pi/2 - \varphi_{QPSKs})} \sinh(g_{SQ1}z) \right] \\ & \cdot e^{j[2\gamma_{SQ1}(|P_{SQ1}|^2 + |P_{SQ2}|^2) - \kappa_{SQ1}/2]z} \\ = & A_s \left[j \sin(\varphi_{QPSKs}) e^{g_{SQ1}z} \right. \\ & \left. + \cos(\varphi_{QPSKs}) e^{-g_{SQ1}z} \right] \\ & \cdot e^{j\{2\pi f_c t + [2\gamma_{SQ1}(|P_{SQ1}|^2 + |P_{SQ2}|^2) - \kappa_{SQ1}/2]z\}} \\ \approx & jA_s \sin(\varphi_{QPSKs}) e^{g_{SQ1}z} \\ & \cdot e^{j\{2\pi f_c t + [2\gamma_{SQ1}(|P_{SQ1}|^2 + |P_{SQ2}|^2) - \kappa_{SQ1}/2]z\}} \end{aligned} \quad (7)$$

where $e^{g_{SQ1}z} \gg e^{-g_{SQ1}z}$ is adopted to obtain the final expression of $S(z, t)$. It is easy to prove that the term $\sin(\varphi_{QPSKs})$

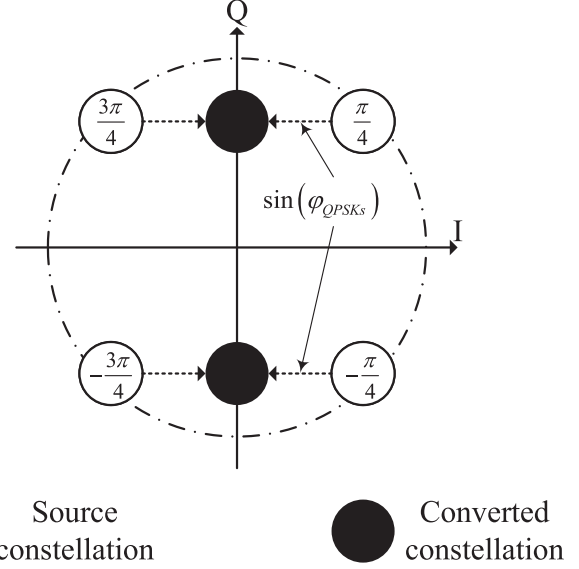


Fig. 8. Constellation conversion from QPSK to BPSK of Q branch [i.e., $S(0, t) \rightarrow S(z, t)$].

describes the Q branch of $S(0, t)$ with two opposite values. Thus, four phases of the produced signal $S(z, t)$ after Stage 1 could be approximated to only two discrete phases with the difference of π as Fig. 8 shows, which could also be considered as a BPSK signal.

During all the demonstration in [31], [35], [36], [37], [38], [39], a phase shift of $\pi/2$ was attached to $S(0, t)$ to discriminate the other I branch of $S(0, t)$. This practice can be formulated similarly to (7):

$$\begin{aligned} S(z, t) = & \left[A_s e^{j(2\pi f_c t + \varphi_{QPSKs} + \pi/2)} \cosh(g_{SQ1}z) \right. \\ & \left. + jA_s e^{j(2\pi f_c t + \pi/2 - \varphi_{QPSKs} - \pi/2)} \sinh(g_{SQ1}z) \right] \cdot \\ & e^{j[2\gamma_{SQ1}(|P_{SQ1}|^2 + |P_{SQ2}|^2) - \kappa_{SQ1}/2]z} \\ = & A_s \left[j \cos(\varphi_{QPSKs}) e^{g_{SQ1}z} \right. \\ & \left. - \sin(\varphi_{QPSKs}) e^{-g_{SQ1}z} \right] \\ & \cdot e^{j\{2\pi f_c t + [2\gamma_{SQ1}(|P_{SQ1}|^2 + |P_{SQ2}|^2) - \kappa_{SQ1}/2]z\}} \\ \approx & jA_s \cos(\varphi_{QPSKs}) e^{g_{SQ1}z} \\ & \cdot e^{j\{2\pi f_c t + [2\gamma_{SQ1}(|P_{SQ1}|^2 + |P_{SQ2}|^2) - \kappa_{SQ1}/2]z\}} \end{aligned} \quad (8)$$

Equation (8) seems to tell us that the format conversion of the I branch could share the same structure as Fig. 6. Unfortunately, the shared structure cannot convert the I and Q branch simultaneously unless split $S(0, t)$ to two paths with the phase shift of 0 and $\pi/2$ respectively then double the structure in Fig. 6 for each path to achieve simultaneous format conversion. For a high-speed system, converting the two branches simultaneously is certainly more effective compared with separately converting the two branches in different time slots. According to the statement in

Stage 1, the DFWM process must be stimulated by phase-locked pumps and signal, doubling the structure means doubling the phase-locking circuits to maintain the phase-locking requirement of each path, which costs expensively. Note that the DFWM process of the I branch's format conversion in Section III-B1 does not need to be phase locked, therefore, in this work, we adopt different format conversion methods for the I and Q branch instead of $\pi/2$ phase shift in the references.

b) Stage 2: In Fig. 7, at the second stage, a usual FWM is stimulated by the phase-locked $P_{SQ3}(0, t)$ and $P_{SQ4}(0, t)$ with $S(z, t)$. An idle signal described as $I_{SQ}(z, t)$ will be generated after the stage at frequency $f_c + (f_c + 3\Delta f_2) - (f_c + \Delta f_2) = f_c + 2\Delta f_2$, and $P_{SQ3}(z, t)$, $P_{SQ4}(z, t)$, $S(z, t)$ and $I_{SQ}(z, t)$ should satisfy the CAEs given by:

$$\begin{cases} \frac{dP_{SQ4}}{dz'} = j\gamma_{SQ2} \left[(|P_{SQ4}|^2 + 2|P_{SQ3}|^2) P_{SQ4} \right] \\ \frac{dS}{dz'} = j2\gamma_{SQ2} \left[(|P_{SQ3}|^2 + |P_{SQ4}|^2) S \right. \\ \quad \left. + \overline{P_{SQ4}P_{SQ3}I_{SQ}} e^{j\Delta k_{SQ2}z'} \right] \\ \frac{dP_{SQ3}}{dz'} = j\gamma_{SQ2} \left[(|P_{SQ3}|^2 + 2|P_{SQ4}|^2) P_{SQ3} \right] \\ \frac{dI_{SQ}}{dz'} = j2\gamma_{SQ2} \left[(|P_{SQ3}|^2 + |P_{SQ4}|^2) I_{SQ} \right. \\ \quad \left. + P_{SQ4}S\overline{P_{SQ3}} e^{-j\Delta k_{SQ2}z'} \right] \end{cases} \quad (9)$$

In (9), assume that $|P_{SQ3}|^2$ or $|P_{SQ4}|^2 \gg |S|^2$ or $|I_{SQ}|^2$, $I_{SQ}(0, t) = 0$ and $\Delta k_{SQ2} = \beta_{P_{SQ3}} + \beta_{I_{SQ}} - \beta_{P_{SQ4}} - \beta_S$. Eq (9) can be solved as:

$$\begin{cases} P_{SQ4}(z, t) = P_{SQ4}(0, t) e^{j\gamma_{SQ2}(|P_{SQ4}|^2 + 2|P_{SQ3}|^2)z'} \\ S(z, t) = S(z, t) \left[\cos(g_{SQ2}z') \right. \\ \quad \left. - \frac{\kappa_{SQ2}}{2g_{SQ2}} \sin(g_{SQ2}z') \right] \\ \quad \cdot e^{j[2\gamma_{SQ2}(|P_{SQ3}|^2 + |P_{SQ4}|^2) + \kappa_{SQ2}/2]z'} \\ P_{SQ3}(z, t) = P_{SQ3}(0, t) e^{j\gamma_{SQ2}(|P_{SQ3}|^2 + 2|P_{SQ4}|^2)z'} \\ I_{SQ}(z, t) = \frac{2\gamma_{SQ2}}{g_{SQ2}} P_{SQ4}(0, t) S(z, t) \overline{P_{SQ3}(0, t)} \\ \quad \cdot \sin(g_{SQ2}z') \\ \quad \cdot e^{j[2\gamma_{SQ2}(|P_{SQ3}|^2 + |P_{SQ4}|^2) - \kappa_{SQ2}/2]z'} \\ \approx j \frac{2\gamma_{SQ2}}{g_{SQ2}} A_{psq3} A_{psq4} A_s \sin(\varphi_{QPSKs}) \\ \quad \cdot e^{g_{SQ1}z} \sin(g_{SQ2}z') \\ \quad \cdot e^{j[2\gamma_{SQ2}(|P_{SQ1}|^2 + |P_{SQ2}|^2) - \kappa_{SQ2}/2]z} \\ \quad \cdot e^{j[2\gamma_{SQ2}(|P_{SQ3}|^2 + |P_{SQ4}|^2) - \kappa_{SQ2}/2]z'} \\ \quad \cdot e^{j[2\pi(f_c + 2\Delta f_2)t + \varphi_{C2}]} \end{cases} \quad (10)$$

where $\kappa_{SQ2} = \gamma_{SQ2}(|P_{SQ3}|^2 - |P_{SQ4}|^2) + \Delta k_{SQ2}$, $g_{SQ2} = \sqrt{4\gamma_{SQ2}^2|P_{SQ3}|^2|P_{SQ4}|^2 + (\kappa_{SQ2}/2)^2}$ and $\varphi_{C2} = \varphi_{Pumpsq4} - \varphi_{Pumpsq3}$ is a constant thanks to the phase-locked pump lasers. As a consequence, all phase information of $S(z, t)$ is copied from f_c to $f_c + 2\Delta f_2$ in $I_{SQ}(z, t)$ after Stage 2.

Similar to Section III-B1, the output signal of the HNLFF will be made up of $P_{SQx}(z, t)$, $x \in \{1, 2, 3, 4\}$, $S(z, t)$ and $I_{SQ}(z, t)$. Filtering $I_{SQ}(z, t)$ and reformulating it as $I_{SQ}(t)$

by using an FD-OP can obtain the other BPSK signal preparing for the next pattern recognition process.

C. Signal Generation

After understanding the format conversion process, we design the signal generation process. In such high speed like the proposed system, for I branch, if $I_{SI}(t)$ was demodulated by a coherent receiver based on Costas loop [41] to trace the initial phase of φ_{Pumpsq} for the local laser, the polar of the demodulated signal corresponding to φ_{BPSKs} would be $\cos(\pi)(-)$, $\cos(0)(+)$, $\cos(\pi)(-)$ and $\cos(0)(+)$. They are different from any branches of $S(0, t)$, i.e., $\cos(\pi/4)(+)$, $\cos(3\pi/4)(-)$, $\cos(-3\pi/4)(-)$ and $\cos(\pi/4)(+)$ of I branch or $\sin(\pi/4)(+)$, $\sin(3\pi/4)(+)$, $\sin(-3\pi/4)(-)$ and $\sin(-\pi/4)(-)$ of Q branch. Although the difference can be corrected by Digital Signal Processor (DSP) after the optical hybrid, the processing is in the electrical domain, which may limit the baud rate caused by electronic bottleneck and is not expected in all-optical systems. In this work, to eliminate the processing in the electrical domain, we design a special constellation mapping in the process of signal generation as displayed in Table I. The Q branch remains while the I branch is replaced by the XOR result of the original I and Q branches. As a result, the polar of the demodulated $I_{SI}(t)$ will be the same as the original I branch of $S(t)$, which completes the format conversion of the I branch.

As for the Q branch, when $\varphi_C1 = \pi/2$ and the power of P_{SQ1} and P_{SQ2} are adjusted appropriately to implement the example in Fig. 8, $I_{SQ}(z, t)$ could be demodulated as $\sin(\pi/4)(+)$, $\sin(3\pi/4)(+)$, $\sin(-3\pi/4)(-)$ and $\sin(-\pi/4)(-)$ approximately, which is the same as the Q branch of $S(t)$. So far, the format conversion of the Q branch is completed.

The constellation mapping in Table I seems a complicated setup way beyond a standard QPSK transmitter. However, the mapping can be implemented during the information generated stage, only a simple XOR operation is added compared to other possible complicated operations of upper layer protocol, e.g. Cyclic Redundancy Check (CRC) and so on. Obviously, this operation does not add any difficulty to the QPSK modulators because there are not any changes in the QPSK driving signals. Since the information data is mandatory to be generated in any case, adding a simple precoded operation during the mandatory information generation can eliminate the post-DSP processing in the electrical domain, which is conducive to constructing all-optical systems.

The target QPSK signal described as $T(0, t) = T(t) = A_t \cdot \exp(j2\pi f_c t + \varphi_{QPSKt})$ also experiences the similar format conversion process with the pump described as $P_{TI}(0, t) = P_{TI}(t) = A_{pti} \exp\{j[2\pi(f_c - \Delta f_2)t + \varphi_{Pumpsq}]\}$ in I branch and four phase-locked high power pumps described as (11) in Q branch.

$$\begin{aligned} P_{TQx}(0, t) &= P_{TQx}(t) \\ &= \begin{cases} A_{ptqx} e^{j[2\pi(f_c + (3-2x)\Delta f_1)t + \varphi_{Pumpsq}]} , x \in \{1, 2\} \\ A_{ptqx} e^{j[2\pi(f_c + (5-2x)\Delta f_2)t + \varphi_{Pumpsq}]} , x \in \{3, 4\} \end{cases} \end{aligned} \quad (11)$$

TABLE I
CONSTELLATION MAPPING FROM THE ORIGINAL SIGNAL TO INPUT SIGNAL

Original I and Q branch		Constellation mapping	Input I and Q branch		Input QPSK phase	Phase after FWM
I	Q		I'	Q'		
0 (-1)	1 (+1)	$I' = I\bar{Q} + \bar{I}Q$	1 (+1)	1 (+1)	$\pi/4$	$\pi/2$
1 (+1)	1 (+1)		0 (-1)	1 (+1)	$3\pi/4$	$-\pi/2$
0 (-1)	0 (-1)	$Q' = Q$	0 (-1)	0 (-1)	$-3\pi/4$	$\pi/2$
1 (+1)	0 (-1)		1 (+1)	0 (-1)	$-\pi/4$	$-\pi/2$

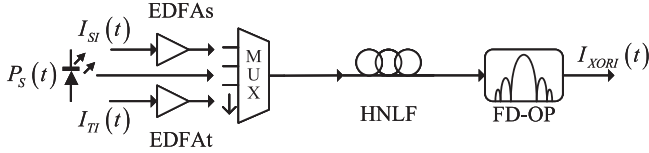


Fig. 9. XOR gate structure of I branch.

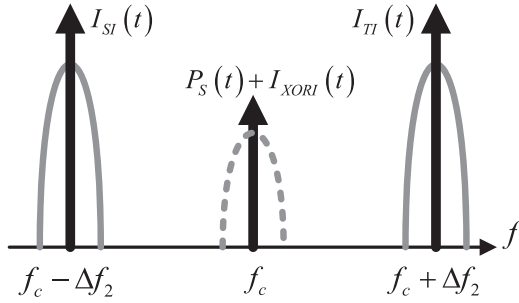


Fig. 10. Frequency allocation of the XOR gate structure in I branch.

Then the converted results are $I_{TI}(t)$ at center frequency $f_c + \Delta f_2$ and $I_{TQ}(t)$ at center frequency $f_c - 2\Delta f_2$.

D. Pattern Recognition

As illustrated in Fig. 2, the pattern recognition process is comprised of an XOR process and a correlation process. At first, the XOR process compares the input sequence and the target pattern sequence, indicating the positions where they are the same. Then the correlation process circularly delays and sums the XOR result so that the highest level could be achieved when the same positions from the XOR process are continuous, which describes the presence and the position of the target pattern sequence in the input sequence.

1) *XOR*: The converted signals $I_{SI}(t)$ and $I_{TI}(t)$ in I branch or $I_{SQ}(t)$ and $I_{TQ}(t)$ in Q branch will be amplified and coupled into an HNLF following with an FD-OP to achieve an XOR gate [42] with a pump described as $P_S(0, t) = P_S(t) = A \exp[j(2\pi f_c t + \varphi_{Pumps})]$, respectively. Because the structure of XOR gates in different branches is the same, we take the I branch as an example illustrated in Fig. 9.

According to Fig. 9, the XOR structure is similar to Stage 1 of the Q branch's format conversion except for the phase-locking requirement of the pumps. Therefore, a DFWM will be stimulated by the amplified $I_{SI}(z, t) = I_{SI}(t)$ at $f_c - \Delta f_2$ and $I_{TI}(z, t) = I_{TI}(t)$ at $f_c + \Delta f_2$ with $P_S(0, t)$ at $f_c - \Delta f_2 + f_c + \Delta f_2 - f_c = f_c$ as Fig. 10 displays. They should satisfy

the CAEs expressed as:

$$\begin{cases} \frac{dI_{SI}}{dz''} = j\gamma_{XORI} \left[(|I_{SI}|^2 + 2|I_{TI}|^2) I_{SI} \right] \\ \frac{dI_{TI}}{dz''} = j\gamma_{XORI} \left[(|I_{TI}|^2 + 2|I_{SI}|^2) I_{TI} \right] \\ \frac{dP_S}{dz''} = j2\gamma_{XORI} \left[(|I_{SI}|^2 + |I_{TI}|^2) P_S \right. \\ \left. + I_{SI}I_{TI}P_S e^{-j\Delta k_{XORI}z''} \right] \end{cases} \quad (12)$$

In (12), except for the description of γ_{XORI} , assume that $|I_{SI}|^2$ or $|I_{TI}|^2 \gg |P_S|^2$ and $\Delta k_{XORI} = 2\beta_{P_S} - \beta_{I_{SI}} - \beta_{I_{TI}}$. According to the same method for solving (1), the solution of (12) can be solved as:

$$\begin{cases} I_{SI}(z, ''t) = I_{SI}(z, t) e^{j\gamma_{XORI}(|I_{SI}|^2 + 2|I_{TI}|^2)z''} \\ I_{TI}(z, ''t) = I_{TI}(z, t) e^{j\gamma_{XORI}(|I_{TI}|^2 + 2|I_{SI}|^2)z''} \\ P_S(z, ''t) = \left\{ P_S(0, t) \cosh(g_{XORI}z'') \right. \\ \left. + j\frac{\kappa_{XORI}}{2g_{XORI}} \sinh(g_{XORI}z'') \right. \\ \left. + j\frac{2\gamma_{XORI}}{g_{XORI}} I_{SI}(z, t) I_{TI}(z, t) \right. \\ \left. \cdot \overline{P_S(0, t)} \sinh(g_{XORI}z'') \right\} \\ \cdot e^{j[2\gamma_{XORI}(|I_{SI}|^2 + |I_{TI}|^2) - \kappa_{XORI}/2]z''} \\ = A \left\{ \left[\cosh(g_{XORI}z'') + j\frac{\kappa_{XORI}}{2g_{XORI}} \right. \right. \\ \left. \cdot \sinh(g_{XORI}z'') \right] + \frac{2\gamma_{XORI}\gamma_{SI}\gamma_{TI}}{g_{XORI}g_{SI}g_{TI}} \\ \cdot A_s^2 A_t^2 \sinh(g_{XORI}z'') \sinh(g_{SI}z) \\ \cdot \sinh(g_{TI}z') e^{j(2\gamma_{SI}|S|^2 - \kappa_{SI}/2)z} \\ \cdot e^{j(2\gamma_{TI}|T|^2 - \kappa_{TI}/2)z'} \\ \cdot e^{j[\pi/2 - (\varphi_{Pumps_i} + \varphi_{Pumps_t} + 2\varphi_{Pumps})]} \\ \cdot e^{j(\varphi_{BPSK_s} + \varphi_{BPSK_t})} \left. \right\} \\ \cdot e^{j(2\pi f_c t + \varphi_{Pumps})} \end{cases} \quad (13)$$

where $\kappa_{XORI} = \gamma_{XORI}(|I_{SI}|^2 + |I_{TI}|^2) + \Delta k_{XORI}$ and $g_{XORI} = \sqrt{4\gamma_{XORI}^2 |I_{SI}|^2 |I_{TI}|^2 - (\kappa_{XORI}/2)^2}$.

According to (2), $\varphi_{BPSK_s} \in \{\pi, 0\}$ and $\varphi_{BPSK_t} \in \{\pi, 0\}$, the summation operation of $\varphi_{BPSK_s} + \varphi_{BPSK_t}$ in (13) will generate two cases of phase: π [demodulated as 0 due to the negative polarity of $\cos(\pi)$] when φ_{BPSK_s} and φ_{BPSK_t} are different and 0 [demodulated as 1 due to the positive polarity of $\cos(0)$] when φ_{BPSK_s} and φ_{BPSK_t} are the same, which describes the XOR logic. Note that there exists an additive term $\cosh(g_{XORI}z'') + j\kappa_{XORI}/(2g_{XORI}) \sinh(g_{XORI}z'')$ in $P_S(z, ''t)$, it could be considered as a local laser added to the BPSK signal of XOR result like the structure of coherent receiver, where the power of

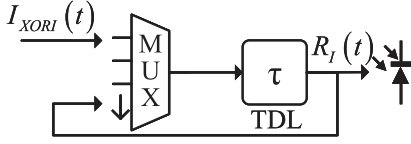


Fig. 11. Correlation structure of I branch.

$P_S(z, '' t)$ can be described as:

$$|P_S(z, '' t)|^2 = A^2 \left\{ 1 + \left(1 + \frac{\kappa_{XORI}^2}{4g_{XORI}^2} \right) \cdot \sinh^2(g_{XORI}z'') + B^2 + 2B \cdot [\cosh(g_{XORI}z'')] \cdot \cos(\varphi_{XORI} + \varphi_{BPSKs} + \varphi_{BPSKt}) + \frac{\kappa_{XORI}}{2g_{XORI}} \sinh(g_{XORI}z'') \cdot \sin(\varphi_{XORI} + \varphi_{BPSKs} + \varphi_{BPSKt}) \right\} \quad (14)$$

where $B = 2\gamma_{XORI}\gamma_{SI}\gamma_{TI}/(g_{XORI}g_{SI}g_{TI})A_s^2A_t^2 \cdot \sinh(g_{XORI}z'') \sinh(g_{SI}z) \sinh(g_{TI}z')$ and $\varphi_{XORI} = (2\gamma_{SI}|S|^2 - \kappa_{SI}/2)z + (2\gamma_{TI}|T|^2 - \kappa_{TI}/2)z' - (\varphi_{Pumps_i} + \varphi_{Pumps_t} + 2\varphi_{Pumps_s}) + \pi/2$. For the determined DFWM process, κ_{XORI} , g_{XORI} , z , z' , z'' , B and φ_{XORI} are all fixed. The XOR result $\varphi_{BPSKs} + \varphi_{BPSKt}$ only owns two discrete phases 0 or π . Thus, it is easy to prove that $P_S(z, '' t)$ can only obtain two different values, which could be seen as a two-level IM signal and indicate the XOR result of $I_{SI}(t)$ and $I_{TI}(t)$ at the center frequency f_c . Filtering $P_S(z, '' t)$ and reformulating as $I_{XORI}(t)$ by an FD-OP can prepare the IM signal for the last correlation process of the I branch.

In Q branch, similar operation will act on $I_{SQ}(t)$ and $I_{TQ}(t)$. We can get $I_{XORQ}(t)$ preparing for the last correlation process of the Q branch.

2) *Correlation*: The correlation in the process of pattern recognition plays the most important role to identify the target pattern from the source signal. Its structure refers to the circular matching in [7] illustrated in Fig. 11. We still take the I branch as an example and the Q branch is the same.

The principle of the optical correlator and circular matching for IM input signals has been explained in detail in [7], [26], [43]. We will just list an example for the results of each loop in the I branch in (15) instead of exploring it. Here we suppose the two levels of IM signals are 0 and 1 and take the sequence of 0011010010 for $S(t)$ and the sequence of 00110100 for $T(t)$ in the I branch as an example.

In (15), the XOR result 1100101101 of sequence 0011010010 and repetitive sequence 1111111111 of $T(t)$ will be cyclically delayed one symbol as 1110010110 by Time Delay Line (TDL) in the correlator structure and then added to the next input XOR result 1100101101, producing 2210111211 then looping the cyclic delay and adding process. After the length of sequence 00110100 (8) loops, the output signal $R_I(t)$ will own $8 + 1 = 9$

levels [0 ~ 8 in (15)], in which the position of the highest level is the last bit's position of sequence 00110100. Therefore, by setting an appropriate threshold as mentioned by Section V to detect the highest output level of $R_I(t)$, this can recognize whether the sequence 00110100 exists in the I branch of $S(t)$ sequence 0011010010 or not and indicate its position in input sequence if exists.

$$\left. \begin{array}{l} \xrightarrow{\text{1st loop}} \\ \text{XOR 0} \end{array} \right\} \begin{array}{l} 1100101101 \xrightarrow{\text{1-symbol delay}} 1110010110 \\ + 1100101101 \xleftarrow{\text{2nd loop}} \\ \text{XOR 0} \\ \downarrow \\ 1221011121 \xleftarrow{\text{1-symbol delay}} 2210111211 \\ \downarrow \\ 1232021131 \xrightarrow{\text{1-symbol delay}} 1123202113 \\ + 0011010010 \xleftarrow{\text{4th loop}} \\ \text{XOR 1} \\ \downarrow \\ 3113421212 \xleftarrow{\text{1-symbol delay}} 1134212123 \\ \downarrow \\ 4213522313 \xrightarrow{\text{1-symbol delay}} 3421352231 \\ + 0011010010 \xleftarrow{\text{6th loop}} \\ \text{XOR 1} \\ \downarrow \\ 1343236224 \xleftarrow{\text{1-symbol delay}} 3432362241 \\ \downarrow \\ 2443337325 \xrightarrow{\text{1-symbol delay}} 5244333732 \\ + 1100101101 \xleftarrow{\text{8th loop}} \\ \text{XOR 0} \\ \downarrow \\ \leftarrow \text{output} \quad 6344434833 \end{array} \quad (15)$$

IV. NUMERICAL SIMULATION CONDITIONS

Although we have explained the principle of the proposed system, in theory, there are still two problems to be discussed before the simulation is set up. One is how to obtain four phase-locked pumps with the signal in the format conversion of the Q branch process. The other is how to generate the repetitive sequence of each target sequence bit directly in the optical domain in the correlation process according to Section III-D2.

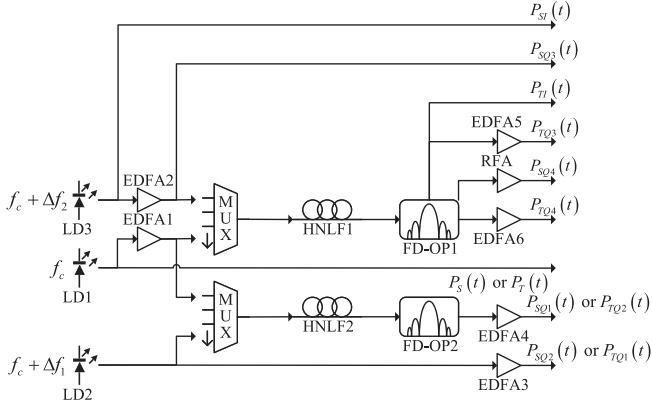


Fig. 12. Pumps generation structure of all pumps.

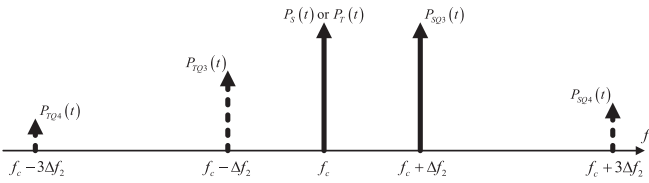


Fig. 13. Frequency allocation of DFWM process over HNLFF1.

A. Solution to Obtain Phase-Locked Pumps

In the experiments of the references, the equidistant pumps were generated by a PM to modulate a Laser Diode (LD) with a Radio Frequency (RF) signal. For high baud rate systems like the proposed system, an ultra-high RF may be used, which is not easily achievable with current electronics. While a PM with such a large electro-optic bandwidth is also too expensive to achieve the high baud rate. Hence, we adopt a pump generation method using phase-insensitive amplifiers (PIAs) with some phase locking units in Tang et al. [44] as illustrated in Fig. 12.

The pumps generated from the PIAs in Fig. 12 are actually the idlers after two DFWM processes stimulated by HNLFF1 and HNLFF2 as Section III-B1 describes. According to [44], in Fig. 12, the generated idlers $P_{TI}(t)$, $P_{SQ4}(t)$ and $P_{TQx}(t)$, $x \in \{3, 4\}$ automatically acquires a certain phase relationship with pumps $P_{SQ4}(t)$ and signals $P_S(t)$ or $P_T(t)$ while $P_{SQ1}(t)$ or $P_{TQ2}(t)$, $P_S(t)$ or $P_T(t)$ and $P_{SQ2}(t)$ or $P_{TQ1}(t)$ is the same. Although filtering, amplifying, and modulating these pumps afterward may split and recombine some pumps, some phase-locking units still can be used to guarantee the requirement of phase-locked pumps as [44] demonstrated. The frequency allocation of these DFWM processes over HNLFF1 and HNLFF2 are illustrated in Figs. 13 and 14.

Note that a Roman Fiber Amplifier (RFA) is adopted here, this is because the frequency of pump $P_{SQ4}(t)$ may be beyond the C+L-band (S-band in fact) which commercial EDFAs like [45] can operate in. A commercial RFA like [46] is a simple choice to operate in the S-band.

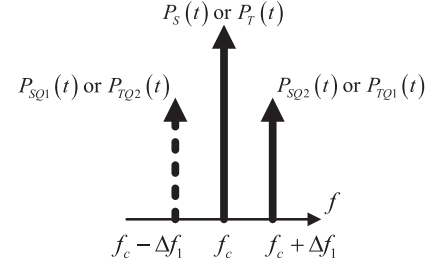


Fig. 14. Frequency allocation of DFWM process over HNLFF2.

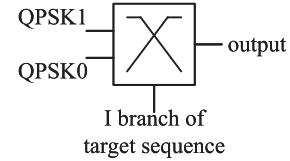


Fig. 15. Optical switch for target pattern sequence repetition.

B. Solution to Generate the Repetitive Sequence

To generate the repetitive sequence, we adopt an optical switch with the target sequence divided into one of the branches controlling as shown in Fig. 15 (take the I branch as an example again). The baud rate of the I branch of a target sequence is $1/[\text{length of I branch of } S(t)]$ multiplied that of $S(t)$ so that each bit of the I branch of $S(t)$ could be repeated to the same length of the I branch of $S(t)$ when QPSK1 (bit 1 modulated in QPSK) or QPSK0 (bit 0 modulated in QPSK) is chosen to the output in the optical domain.

C. Simulation Setup and Parameters

The solutions above to the two problems complete the proposed system. We use VPITransmissionMaker 9.5 (VPI) to simulate the performance of the proposed system at the baud rate of 100GBaud. The complete schematic of our system is shown in Fig. 16.

In the signal generation process, we generate the optical source according to Fig. 12. For three LDs, we choose $A_{LD1}^2 = A_{LD2}^2 = A_{LD3}^2 = 10 \text{ mW}$, $f_c = 193.4145 \text{ THz}$, $\Delta f_1 = 0.5 \text{ THz}$, $\Delta f_2 = 1.5 \text{ THz}$, the linewidth of the LDs is all 100 kHz and $\varphi_{LD1} = \varphi_{LD2} = \varphi_{LD3} = 0$, leading to $\varphi_{Pumps_i} = \varphi_{Pumps_{qx}} = \varphi_{Pumpt_i} = \varphi_{Pumpt_{qx}} = \varphi_{Pumps} = 0$. The amplifiers in Fig. 12 are all set to power-controlled mode with the same output power of 291 mW, resulting in $A_{psi}^2 = A_{pti}^2 = A_{psqx}^2 = A_{ptqx}^2 = 291 \text{ mW}$, $x \in \{1, 2, 3, 4\}$. We adopt the AmpSysOpt module in VPI to implement an EDFA or RFA. The Noise Figure (NF) and Noise Tilt (NT) of all EDFAs are set to 5.5 dB and 0 dB/Hz according to [45], respectively, with the bandwidth of 100 GHz at each pump's center frequency. The bandwidth setting here is the same as assuming an optical filter after each EDFA to remove the out-of-band amplified spontaneous emission (ASE) coming from the EDFA [44]. As for the RFA, the parameters should be -1.0 dB and 0 dB/Hz according to [46]. However, the adopted module AmpSysOpt prohibits us from setting these parameters. Note that the noise

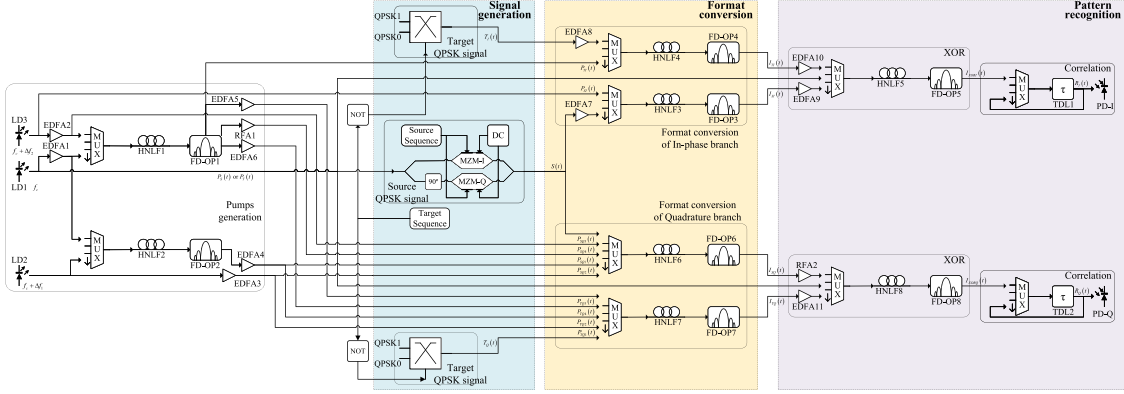


Fig. 16. Complete schematic of our system.

from an RFA is dramatically smaller than an EDFA, we set 0.0 dB and 0 dB/Hz as the NF and NT for the RFAs.

For the preparation of QPSK signals, firstly, the QPSK source sequence is distributed into the I branch and the Q branch. Then they are mapped to the I and Q input sequence as Table I displays. Next, two 100GBaud Double Polarity Not Return to Zero (DPNRZ) signals of the I and Q branch are generated, adjusted to a rise-time of 0.625 ps and filtered by a 3rd-order Bessel lowpass filter with the bandwidth of 300 GHz, respectively. Finally, the two branches signals are modulated to a QPSK source signal by driving a push_pull IQ Mach-Zehnder external optical Modulator (IQ-MZM) with 35 dB extinction ratio, 0 dB insertion loss, and $V_{\pi DC} = V_{\pi RF} = 8$ V at the null-point bias. The target pattern QPSK signals are repetitively generated according to Fig. 15 with the same preparation and IQ-MZMs as that of the source signal.

In the pattern recognition process, the input power of the converted signals in the XOR process is adjusted to 20 mW by an EDFA, i.e., $|I_{SI}|^2 = |I_{TI}|^2 = |I_{SQ}|^2 = |I_{TQ}|^2 = 20$ mW. The noise parameters of these EDFAs are set to the same as those in the signal generation process, only the bandwidth is modified to 300 GHz. Note that there is also an RFA adopted here to operate in S-band, the noise parameters are also the same as 0.0 dB and 0 dB/Hz, and the bandwidth is also modified to 300 GHz.

All HNLFs adopted in different processes have the same length of 200 m and are based on the commercial product NL-1550-Zero [47] from Yangtze Optical Fibre and Cable Joint Stock Limited Company (YOFC) [47] with zero dispersion at 1550 nm, $0.03\text{ps}/(\text{nm}^2 \cdot \text{km})$ dispersion slope, $13.23 \mu\text{m}^2$ effective core area and the nonlinear Kerr parameter $n_2 = 3.264 \times 10^{-20} \text{m}^2/\text{W}$. In terms of all FD-OPs adopted in different processes, we configure them as a 1-order Gaussian bandpass filter. The bandwidth of FD-OPs in the signal generation process is the same as the source baud rate, i.e., 100 GHz, and 3 times as wide as the source baud rate, i.e., 300 GHz in other processes.

As for the PDs to detect the optical pattern recognition results, both of them are PIN-model as [48] defines. The responsivity is 0.65 A/W. Detecting current of them will be influenced

 TABLE II
 PARAMETERS IN SIMULATION SETUP

Parameter	Value
$A_{LD1}^2 = A_{LD2}^2 = A_{LD3}^2$	10mW
f_c	193.4145THz (1550nm)
Linewidth of LDs	100kHz
$\varphi_{LD1} = \varphi_{LD2} = \varphi_{LD3}$	0
Δf_1	0.5THz
Δf_2	1.5THz
$A_{psi}^2 = A_{pti}^2 = A_{psqx}^2 = A_{ptqx}^2$	291mW
Data baud rate	100GBaud
Rise-time of two branches	0.625ps
Filter type of two branches	3rd-order Bessel lowpass
Bandwidth of two branches	300GHz
Type of IQ-MZMs	push_pull
Extinction ratio of IQ-MZMs	35dB
Insertion loss of IQ-MZMs	0dB
$V_{\pi CD} = V_{\pi RF}$	8V
DC bias of IQ-MZMs	Null point
$ I_{SI} ^2 = I_{TI} ^2 = I_{SQ} ^2 = I_{TQ} ^2$	20mW
NF of EDFAs	5.5dB
NF of RFAs	0.0dB
NT of EDFAs and RFAs	0dB/Hz
Length of HNLFs	200m
Type of HNLFs	YOFC NL-1550-Zero
Dispersion of HNLFs	0ps/(nm · km) (1550nm)
Dispersion slope of HNLFs	0.03ps/(nm · km)
Effective core area of HNLFs	$13.23 \mu\text{m}^2$
n_2	$3.264 \times 10^{-20} \text{m}^2/\text{W}$
Filter type of FD-OPs	1st-order Gaussian bandpass
Bandwidth of FD-OPs in signal generation process	100GHz
Bandwidth of FD-OPs in other processes	300GHz
Model of PDs	PIN
Responsivity of PDs	0.65A/W
Dark current of PDs	5nA
Thermal noise of PDs	$10^{-12} \text{A}/\sqrt{\text{Hz}}$
Shot noise of PDs	On
Bandwidth of PDs	100GHz

by the sum of the dark current of 5nA, the thermal noise of $10^{-12} \text{A}/\sqrt{\text{Hz}}$, and shot noise. Moreover, the PD model owns a bandwidth of 100 GHz with DC-coupled.

A summary of the parameters abovementioned is presented in Table II. Unless stated explicitly in corresponding texts, all these parameters listed in Table II are adopted throughout this paper.

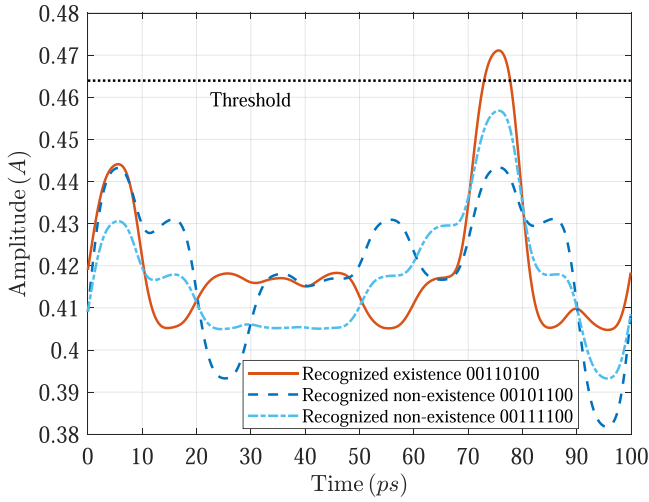


Fig. 17. Recognition result of I branch for short assigned sequences.

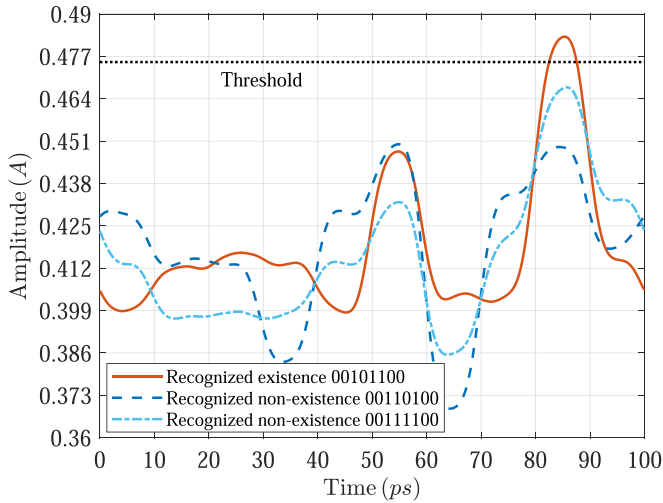


Fig. 18. Recognition result of Q branch for short assigned sequences.

V. SIMULATION RESULTS AND ANALYSIS

Based on the theoretical analysis in Section III and by making use of the system setup and its corresponding operating parameters in Section IV, in this section, we prove the QPSK signal's pattern recognizing feasibility of I branch and Q branch, the arbitrary target patterns processing ability of I branch and Q branch, and how to recognize the target pattern in source QPSK sequence of our proposed system, respectively.

Firstly, we assign a sequence with a length of 20 bits, i.e., 10 symbols for QPSK modulation, to demonstrate the feasibility of our system. The sequence of $S(t)$ is assigned to 01001011001101001000 for QPSK modulation while the target pattern sequence to be recognized is 0000111001110000. Thus, the target pattern of the I branch and the Q branch is 00110100 and 00101100, respectively. The sequence to find the target pattern for the I branch and the Q branch is 0011010010 and 1001011000, respectively. $R_I(t)$ and $R_Q(t)$ will demonstrate the highest level at the last bit of their respective target pattern, as illustrated in Figs. 17 and 18. We also assign two additional

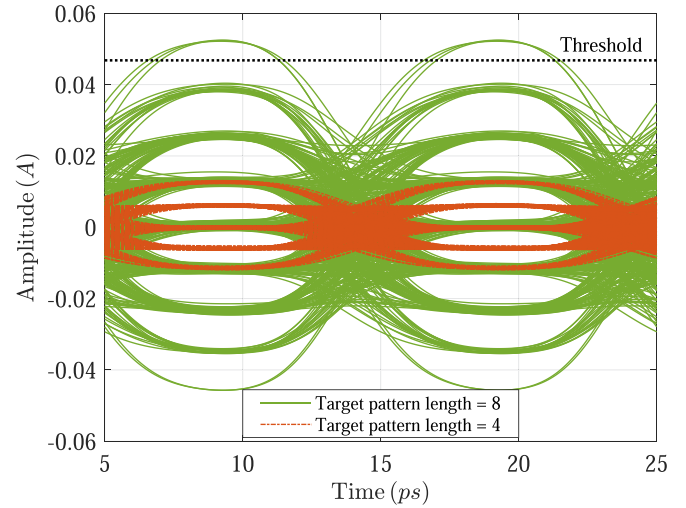


Fig. 19. Recognition result of I branch for long random sequence.

cases of target pattern sequences, i.e., 0000110110110000 and 0000111111110000, which swaps the position of two adjacent bits or only changes one bit, leading to them not existing in $S(t)$ sequence. $R_I(t)$ and $R_Q(t)$ is also illustrated in Figs. 17 and 18. The recognition results could not reach the highest level abovementioned at any moment, therefore, either I or Q branch of 0000110110110000 and 0000111111110000 does not exist in $S(t)$, which proves the feasibility of our system.

In Section III-A, we have taken no account of SRS influence. To verify it, here, we simulate Figs. 17 and 18 again by using the common values of SRS for the HNLFF model in VPI. As a result, except for the changes in amplitude, recognition results are almost the same as Figs. 17 and 18. It turns out that SRS has little effect on the recognition results, which proves the correctness of our assumption in Section III-A.

Next, note that the threshold to judge the highest level in Figs. 17 or 18 plays an important role in the recognition result, we develop a threshold-setting method and employ it to prove the ability to recognize arbitrary target patterns as well. A 1000-bit pseudo-random sequence of $S(t)$ and two different lengths of target pattern sequences 16 (0000111001110000) and 8 (11100111) are assigned. Since there may be too many highest levels with slightly different amplitudes during the whole time window to be recognized, clearly as shown in Figs. 17 or 18, we adopt eye diagrams of the AC component of $R_I(t)$ or $R_Q(t)$ to show the highest level and the system performance as explored in Figs. 19 and 20. The two figures prove the number of levels (8+1 and 4+1) analyzed in Section III. Moreover, three green solid lines at the highest level reveal that the proposed system could recognize the target pattern sequence with the length of 16 simultaneously when there are several target sequences in the source QPSK signal. In addition, although the noise has impacts on the system to a certain extent, distinguishable opening between two adjacent levels in the eye diagram can still make sure a right judgment of the highest level of $R_I(t)$ or $R_Q(t)$, which makes the recognition threshold able to set. For Figs. 19 or 20, the recognition threshold could be set to

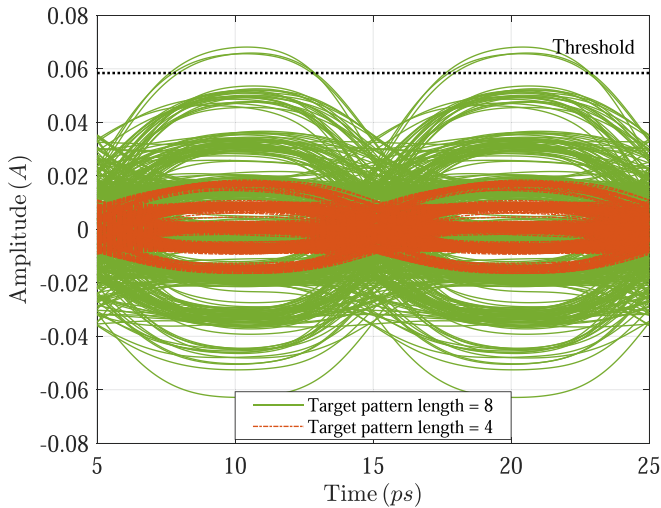


Fig. 20. Recognition result of Q branch for long random sequence.

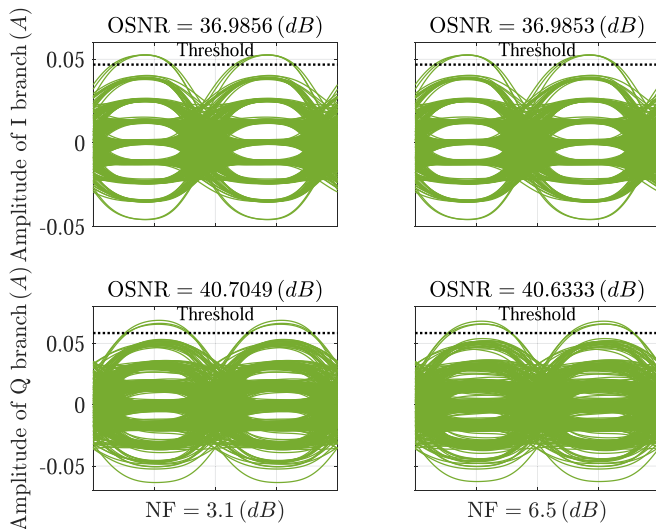


Fig. 21. Recognition result of I and Q branch with NF changing.

the average of the highest level and the second highest level at optimal sampling time, which is about 0.0468 A for the I branch and 0.0584 A for Q branch above the average amplitude. When describing the threshold in absolute amplitude, it is about 0.464 A and 0.475 A as shown in Figs. 17 or 18.

Although we adopt the typical values of some commercial components' noise, e.g. EDFAs, in practice, noise may change away from its typical values. Therefore, we change the parameter NF to see the resilience to the noise of our proposed system. The values start from 3.1 dB because of the quantum limit and end with 6.5 dB according to the maximum NF in [45]. We only display the results in these two values as Fig. 21 due to the slight difference between the results. Also, a common metric named Optical Signal-to-Noise Ratio (OSNR) before the PD is listed simultaneously. In Fig. 21, when NF changes, the changes of OSNR are too small to observe the performance like the usual communication systems. For the I branch, the eye diagram is still maintained, resulting in the set threshold being maintained.

The results reveal that the pattern recognition of the I branch can be immune to the noise, which further proves the advantage of different structures between the I and Q branch. While for the Q branch, the opening in the middle level of the eye diagram is getting smaller with the NF growing. This phenomenon demonstrates that the Q branch is vulnerable to noise. However, the opening between the highest and the second highest level remains, resulting in the threshold remaining, which indicates that the Q branch of our proposed system can only fight against the noise to a certain extent.

Fig. 21 demonstrates the resilience to a certain extent of the noise but it has much to do with the EDFAs' power. Fig. 22 illustrates the changes of I and Q branch eye diagrams along with the power from 275 mW to 305 mW. The four similar eye diagrams of the I branch still state its immunity to the power while the four different eye diagrams of the Q branch describe the influence of different power settings. During the power changes in 30 mW, the eye diagrams close so that we cannot decide the right threshold to judge the highest level. The possible reason for this phenomenon is the phase matching of the FWM processes. For the I branch, the phase matching parameter κ_{SI} in (2) is associated with the power of S and Δk_{SI} . Only three wavelengths participated in the FWM make Δk_{SI} mainly affect κ_{SI} . Therefore, κ_{SI} is not sensitive to the changes in the power of S , which demonstrates the immune results of the I branch. As for the Q branch, κ_{SQ1} in (5) and κ_{SQ2} in (10) is related to too many variables, such as the power of P_{SQ1} , Δk_{SQ1} , Δk_{SQ2} , etc. Too many wavelengths participated in the FWM intuitively make the phase matching more sensitive. As a consequence, the results degrade just within a small range of power changing, which inspires us that the power of EDFAs or RFAs needs to be configured carefully (i.e. 291 mW in this work) to achieve resilience to some noise. Based on the lack of phase matching, the processing speed of the system can be limited as well. In addition, after our test, the influence of NT is little thanks to the bandwidth setting of EDFAs and the influence of PDs' noise is not as evident as NF, hence, we will leave them out in this work.

Then, after the respective recognition of the I branch or Q branch, we have to recognize the QPSK target pattern in the source QPSK sequence. Note that the target pattern to be recognized must be continuous in the source QPSK signal, therefore, the highest level of the I branch and Q branch should exist in the same position in the recognition results of two branches as seen in Fig. 23. Then the position of the last bit of the target pattern in the source QPSK sequence is double the position of the highest level of the I branch or Q branch.

Finally, we take a real Transmission Control Protocol (TCP) Ethernet frame captured from WIRESHARK 3.4.1 as an example to recognize the splicing of the Media Access Control (MAC) head (14 Bytes), Internet Protocol (IP) head (20 Bytes) and TCP head (20 Bytes). The total bits to be recognized is $(14 + 20 + 20) \times 8 = 432$ bits, therefore, if the splicing is matched, there will be the highest level at the position of the 216th bit. Fig. 24 illustrates the recognition result. To prevent too-long simulation time or even the out-of-memory error popping up from VPI because of too many samples input, we

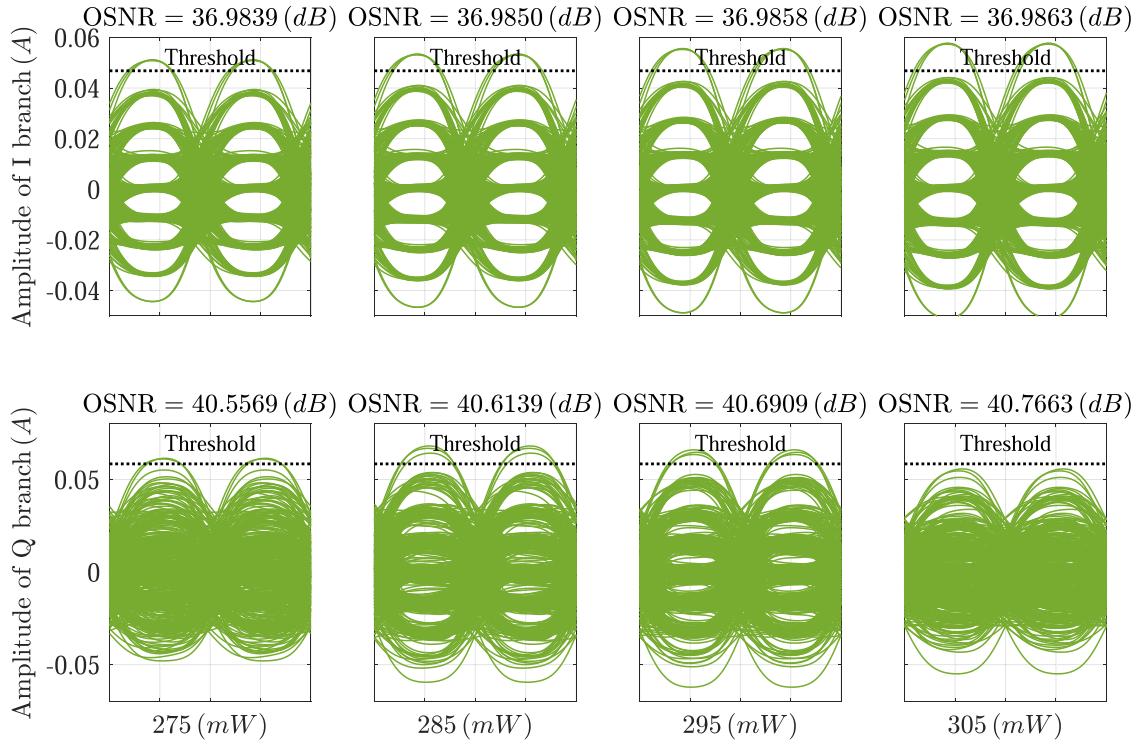


Fig. 22. Recognition result of I and Q branch with power changing.

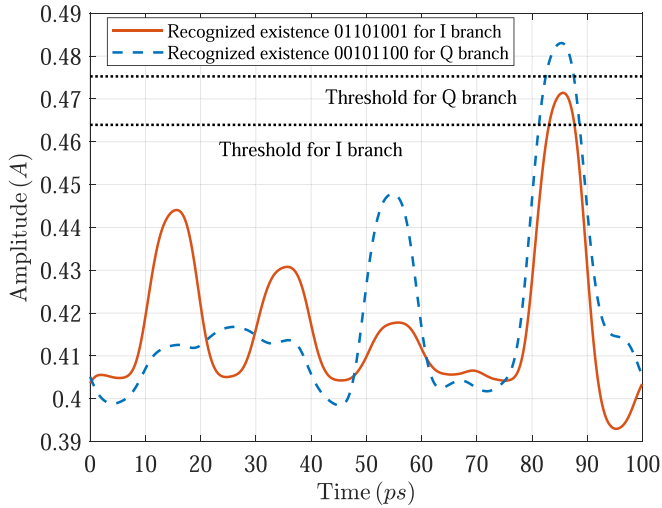


Fig. 23. Recognition result for QPSK matching sequence.

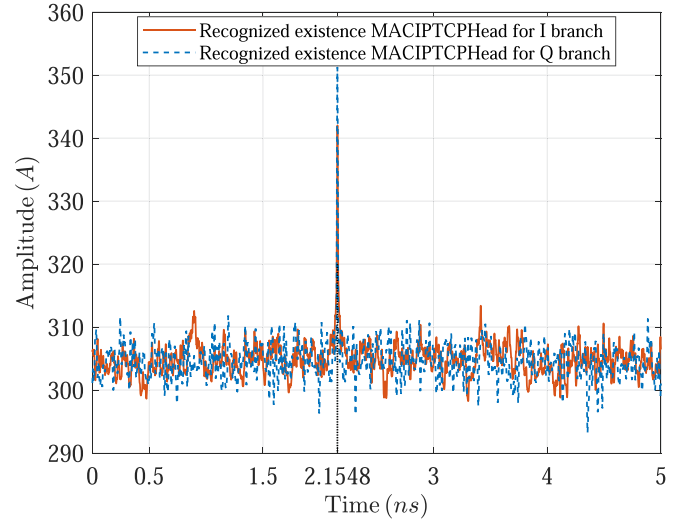


Fig. 24. Recognition result for real IP package sequence.

truncate the real frame with the length of 1514 Bytes (12112 bits) to a binary stream with a length of 1000 bits from the start of the frame. As a result, the time window of the truncated frame will change to $1000/(2 \times 100 \times 10^9) \times 10^9 = 5\text{ns}$ as shown in Fig. 24. The highest level locates at 2.1548 ns as Fig. 24 shows, which is right the last bit's position of the splicing to be recognized. The matched result of a real Ethernet frame further reveals that our proposed system could recognize the whole splicing sequence up to 432 bits and is promisingly applied in optoelectronic firewalls.

VI. CONCLUSION

In this work, a 100 GBaud baud rate pattern recognition system that could recognize arbitrary target patterns of QPSK signals has been proposed. We elaborated the operating principle in detail and VPI simulation results demonstrated that the system can recognize arbitrary target patterns and the baud rate of the processed signal can be up to 100 GBaud, which describes 200 Gbps that was expected to achieve large-scale commercial deployment in the 5G era of source QPSK signals. Moreover, the

format conversion process of the Q branch could be applied to QAM signals to perform the QAM to PAM format conversion, which is expected to achieve QAM pattern recognition in future work. However, although two branches of the proposed system could be recognized respectively, the recognition of the whole target pattern still relies on the decision of whether the highest level is in the same bit or not in the electrical domain, which may require a complicated synchronization technology for the real experimental implementation in the future.

REFERENCES

- [1] K. Kitayama et al., "Security in photonic networks: Threats and security enhancement," *J. Lightw. Technol.*, vol. 29, no. 21, pp. 3210–3222, 2011.
- [2] M. P. Fok, Z. Wang, Y. Deng, and P. Prucnal, "Optical layer security in fiber-optic networks," *IEEE Trans. Inf. Forensics Secur.*, vol. 6, no. 3, pp. 725–736, Sep. 2011.
- [3] D. Dahan and U. Mahlab, "Security threats and protection procedures for optical networks," *IET Optoelectron.*, vol. 11, no. 5, pp. 186–200, 2017.
- [4] D. Wang, Z. Wu, M. Zhang, and X. Tang, "Multifunctional all-optical signal processing scheme for wavelength-division-multiplexing multicast, wavelength conversion, format conversion, and all-optical encryption using hybrid modulation format exclusive-OR gates based on four-wave mixing in highly nonlinear fiber," *Appl. Opt.*, vol. 57, no. 7, pp. 1562–1568, 2018.
- [5] P. Y. Ma, B. Wu, B. J. Shastri, A. N. Tait, P. Mittal, and P. R. Prucnal, "Steganographic communication via spread optical noise: A link-level eavesdropping resilient system," *J. Lightw. Technol.*, vol. 36, no. 23, pp. 5344–5357, Dec. 2018.
- [6] Z. Yang, J. Ke, Q. Zhuge, W. Hu, and L. Yi, "Coherent chaotic optical communication of 30 Gb/s over 340-km fiber transmission via deep learning," *Opt. Lett.*, vol. 47, no. 11, pp. 2650–2653, 2022.
- [7] R. P. Webb et al., "All-optical header processing in a 42.6 Gb/s optoelectronic firewall," *IEEE J. Sel. Topics Quantum Electron.*, vol. 18, no. 2, pp. 757–764, Mar./Apr. 2012.
- [8] L. Yu, L. Xin, T. Ying, S. Zicheng, and H. Shanguo, "Binary sequence matching system based on cross-phase modulation and four-wave mixing in highly nonlinear fibers," *Opt. Eng.*, vol. 59, no. 10, pp. 1–17, 2020.
- [9] K. Xu, X. Li, Y. Tang, and C. Yuan, "Serial-parallel combined all optical sequence matching system using highly nonlinear fibers for photonic firewall," *Optik*, vol. 244, pp. 1–11, 2021.
- [10] A. Almaiman et al., "Demonstration of QPSK data correlation and equalization using a tunable optical tapped delay line based on orbital angular momentum mode delays," *Opt. Commun.*, vol. 503, pp. 1–6, 2022.
- [11] F. Alishahi et al., "Demonstration of a tunable optical correlation of a 10–15 Gbaud QPSK data signal using nonlinear wave mixing at a remotely controlled node," in *Proc. IEEE Photon. Conf.*, 2021, pp. 1–2.
- [12] F. Alishahi et al., "Experimental demonstration of remotely controlled and powered tunable optical 2–4 taps correlator of a 20–100 Gbit/s QPSK channel based on laser-delivered bias and control signals," in *Proc. Opt. Fiber Commun. Conf. Exhib.*, 2021, pp. 1–3.
- [13] M. Ziyadi et al., "Tunable optical correlator using an optical frequency comb and a nonlinear multiplexer," *Opt. Exp.*, vol. 22, no. 1, pp. 84–89, 2014.
- [14] Q. Zhang, X. Gong, and L. Guo, "All-optical pattern recognition of QPSK signals for high speed optoelectronic firewalls," in *Proc. Asia Commun. Photon. Conf. Int. Conf. Inf. Photon. Opt. Commun.*, 2020, pp. 1–3.
- [15] X. Gong, Q. Zhang, X. Zhang, R. Xuan, and L. Guo, "Security issues and possible solutions of future-oriented optical access networks for 5G and beyond," *IEEE Commun. Mag.*, vol. 59, no. 6, pp. 112–118, Jun. 2021.
- [16] R. P. Webb et al., "All-optical binary pattern recognition at 42 Gb/s," *J. Lightw. Technol.*, vol. 27, no. 13, pp. 2240–2245, 2009.
- [17] J. M. Martinez, J. Herrera, F. Ramos, and J. Marti, "All-optical address recognition scheme for label-swapping networks," *IEEE Photon. Technol. Lett.*, vol. 18, no. 1, pp. 151–153, Jan. 2006.
- [18] M. Aljada, K. Alameh, B. Ha Lee, Y. Tak Lee, K. Im, and S. J. Baik, "Experimental demonstration of a dynamic 10 Gbit/s WDM header/label recognition structure," *IEEE J. Sel. Topics Quantum Electron.*, vol. 13, no. 5, pp. 1560–1567, Sep./Oct. 2007.
- [19] D. F. Geraghty, R. Salem, M. A. Foster, and A. L. Gaeta, "A simplified optical correlator and its application to packet-header recognition," *IEEE Photon. Technol. Lett.*, vol. 20, no. 7, pp. 487–489, Apr. 2008.
- [20] G. Cincotti, "Full optical encoders/decoders for photonic IP routers," *J. Lightw. Technol.*, vol. 22, no. 2, pp. 337–342, Feb. 2004.
- [21] O. Moriwaki, T. Kitoh, T. Sakamoto, and A. Okada, "Novel PLC-Based optical correlator for multiple phase-modulated labels," *IEEE Photon. Technol. Lett.*, vol. 17, no. 2, pp. 489–491, Feb. 2005.
- [22] I. Kang et al., "All-optical byte recognition for 40-Gb/s phase-shift-keyed transmission using a planar-lightwave-circuit passive correlator," *IEEE Photon. Technol. Lett.*, vol. 20, no. 12, pp. 1024–1026, Jun. 2008.
- [23] M. S. Rasras et al., "A programmable 8-bit optical correlator filter for optical bit pattern recognition," *IEEE Photon. Technol. Lett.*, vol. 20, no. 9, pp. 694–696, May 2008.
- [24] R. Kibria, L. A. Bui, A. Mitchell, and M. W. Austin, "(IPC) a photonic correlation scheme using FWM with phase management to achieve optical subtraction," *IEEE Photon. J.*, vol. 5, no. 6, pp. 5502209–5502209, Dec. 2013.
- [25] European-Commission, "Wirespeed security domains using optical monitoring," 2006. [Online]. Available: <https://cordis.europa.eu/project/id/033847>
- [26] J. Guo, X. Li, Y. Tang, L. Zhang, T. Gao, and S. Huang, "An all-optical binary pattern recognition system applied in photonic firewall based on VPI simulation," in *Proc. 24th Opto Electron. Commun. Conf. Int. Conf. Photon. Switching Comput.*, 2019, pp. 1–3.
- [27] X. Li, J. Guo, Y. Tang, Y. Liu, H. Wang, and S. Huang, "Parallel all-optical binary recognition system for short sequence detection applied in photonic firewall," in *Proc. Asia Commun. Photon. Conf.*, 2019, pp. 1–3.
- [28] M. R. Chitgarha et al., "Coherent correlator and equalizer using a reconfigurable all-optical tapped delay line," *Opt. Lett.*, vol. 38, no. 13, pp. 2271–2273, 2013.
- [29] A. N. Willner et al., "Scalable and reconfigurable optical tapped-delay-line for multichannel equalization and correlation using nonlinear wave mixing and a kerr frequency comb," *Opt. Lett.*, vol. 43, no. 22, pp. 5563–5566, 2018.
- [30] G. P. Agrawal, *Nonlinear Fiber Optics*, 5th ed. Boston: San Francisco, CA, USA: Academic Press, 2013.
- [31] F. D. Ros, K. Dalgaard, L. Lei, J. Xu, and C. Peucheret, "QPSK-to-2× BPSK wavelength and modulation format conversion through phase-sensitive four-wave mixing in a highly nonlinear optical fiber," *Opt. Exp.*, vol. 21, no. 23, pp. 28743–28750, 2013.
- [32] Y. H. Wen, J. W. Ho, and K. M. Feng, "Phase transparent demultiplexer for QPSK signal based on nonlinear response in a double-pass architecture," *IEEE Photon. J.*, vol. 8, no. 4, pp. 1–7, Aug. 2016.
- [33] M. E. Marhic, *Fiber Optical Parametric Amplifiers, Oscillators and Related Devices*. New York, NY, USA: Cambridge Univ. Press, 2007.
- [34] COHERENT, "WaveShaper 1000 a programmable optical filter," 2023. [Online]. Available: <https://ii-vi.com/product/waveshaper-1000a-programmable-optical-filter/>
- [35] R. P. Webb, J. M. Dailey, R. J. Manning, and A. D. Ellis, "Phase discrimination and simultaneous frequency conversion of the orthogonal components of an optical signal by four-wave mixing in an SOA," *Opt. Exp.*, vol. 19, no. 21, pp. 20015–20022, 2011.
- [36] M. J. Power, R. P. Webb, and R. J. Manning, "All-optical phase discrimination using SOA," *Opt. Exp.*, vol. 21, no. 22, pp. 25664–25669, 2013.
- [37] F. Da Ros, K. Dalgaard, Y. Fukuchi, J. Xu, M. Galili, and C. Peucheret, "Simultaneous QPSK-to-2× BPSK wavelength and modulation format conversion in PPLN," *IEEE Photon. Technol. Lett.*, vol. 26, no. 12, pp. 1207–1210, Jun. 2014.
- [38] R. P. Webb, M. Power, and R. J. Manning, "Phase-sensitive frequency conversion of quadrature modulated signals," *Opt. Exp.*, vol. 21, no. 10, pp. 12713–12727, 2013.
- [39] M. Baillet, M. Gay, C. Peucheret, J. Michel, and T. Chartier, "Phase quadrature discrimination based on three-pump four-wave mixing in nonlinear optical fibers," *Opt. Exp.*, vol. 24, no. 23, pp. 26930–26941, 2016.
- [40] K. A. Croussore and G. Li, "Phase-regenerative wavelength conversion for BPSK and DPSK signals," *IEEE Photon. Technol. Lett.*, vol. 21, no. 2, pp. 70–72, Jan. 2009.
- [41] J. K. Perin, A. Shastri, and J. M. Kahn, "Coherent data center links," *J. Lightw. Technol.*, vol. 39, no. 3, pp. 730–741, Feb. 2021.

- [42] J. Wang, Q. Sun, and J. Sun, "All-optical 40 Gbit/s CSRZ-DPSK logic XOR gate and format conversion using four-wave mixing," *Opt. Exp.*, vol. 17, no. 15, pp. 12555–12563, 2009.
- [43] M. C. Hauer et al., "Optically assisted internet routing using arrays of novel dynamically reconfigurable FBG-Based correlators," *J. Lightw. Technol.*, vol. 21, no. 11, pp. 2765–2778, 2003.
- [44] R. Tang, P. S. Devgan, V. S. Grigoryan, P. Kumar, and M. Vasilyev, "In-line phase-sensitive amplification of multi-channel CW signals based on frequency nondegenerate four-wave-mixing in fiber," *Opt. Exp.*, vol. 16, no. 12, pp. 9046–9053, 2008.
- [45] C. Amonics, "L EDFA Band," 2021. [Online]. Available: <https://www.amonics.com/product/2>
- [46] Amonics Ltd., "Discrete raman amplifier," 2021. [Online]. Available: <https://www.amonics.com/product/84>
- [47] YOFC, "Products-high nonlinear optical fibre (HNLF)" 2023. [Online]. Available: <http://en.yofc.com/view/2353.html>
- [48] COHERENT, "100 GHz single high-speed photodetector," 2023. [Online]. Available: <https://ii-vi.com/product/100-ghz-single-high-speed-photodetector/>